were determined as $I_{tot} = C(F_V - B_V) + 2(F_H - B_H)$, $A_n = [C(F_V - B_V) - (F_H - B_H)]/I_{tot}$. Abbreviations: I_{tot}, total relative intensity; C, calibration ratio from the horizontal to the vertical fluorescence channel; F_V and F_H, vertical and horizontal polarized fluorescence signals, respectively; B_V and B_H, vertical and horizontal polarized background, respectively; A_n, resulting anisotropy. The calibration factor (C) and the background light (B_V and B_H) were determined before each experiment.

4. Randomly dansylated calmodulin has been used for calmodulin-binding studies [reviewed in R. L. Kincaid, M. L. Billingsley, M. Vaughn, *Methods Enzymol.* **159**, 605 (1988)]. For the present experiments, differentially labeled forms of dansylated calmodulin were separated from such a random pool. Calmodulin (Ocean Biologics, Edmonds, WA) was incubated with an approximately fourfold molar excess of dansyl chloride for 45 min at room temperature (10 mg of calmodulin per milliliter, pH 9.0, 50 mM KCl, 20 mM Hepes). Unreacted dansyl was then separated from dansylated calmodulin on a Sephadex G50 column (Piscataway, NJ). Calmodulin species with different amounts of labeling were separated on a high-pressure liquid chromatography hydrophobic interaction column (MP7, Bio-Rad, Richmond, CA) in an ammonium sulfate gradient (1.5 M to 0 M; 100 mM phosphate present in both buffers, pH 7.0). The first peak, which eluted after unlabeled CaM, was designated as CaM^F and used for all studies. Competitive binding studies demonstrated that the affinity of unlabeled calmodulin for CaM kinase is approximately threefold lower than that of CaM^F. The concentration of CaM^F was determined by quantitative amino acid analysis. The concentration of CaM kinase subunits was defined by the concentration of calmodulin binding sites in the preparation.
5. A large amount of rat forebrain CaM kinase (5 mg) was obtained by a three-step purification procedure [H. Schulman, *J. Cell Biol.* **99**, 11 (1984)]. Most of the experiments were repeated with CaM kinase from two separate preparations with similar results.
6. The free Ca^{2+} concentration was initially estimated from Ca^{2+}/EGTA ratios and then determined fluorometrically with the calcium indicator rho-2 [dissociation constant (K_D)-1.0 μM] [A. Minta, J. P. Kao, R. Y. Tsien, *J. Biol. Chem.* **264**, 8171 (1990)].
7. The on-rate of CaM^F to CaM kinase in the absence of ATP was determined by the addition of EGTA and then Ca^{2+} to a highly diluted sample (1.25 nM CaM^F and 1.5 nM CaM kinase subunits). The on-rate was estimated from the time it took for rebinding. The on-rate for CaM^F binding to ATP-exposed CaM kinase was determined by the incubation of high concentrations of CaM^F and CaM kinase subunits (500 nM) in the presence of ATP for 15 s. After this period, glucose (10 mM) and hexokinase (2 U/ml) were added, and then the sample was diluted into the cuvette (final concentrations approximately 5 nM). EGTA was added, and CaM^F was allowed to dissociate for 40 s. The addition of an excess of Ca^{2+} led to the rebinding of CaM^F. The on-rates given in the text are averages of three experiments.
8. Competitive binding studies show that CaM^F has a threefold higher affinity for unphosphorylated CaM kinase than does unlabeled calmodulin. When unlabeled calmodulin is trapped at high Ca^{2+} concentrations in the presence of ATP, it cannot be replaced with CaM^F for long periods of time, indicating that unlabeled CaM, like CaM^F, can be trapped.
9. T. Meyer and L. Stryer, *Proc. Natl. Acad. Sci. U.S.A.* **87**, 3841 (1990).
10. Y. Lai, A. C. Nairn, F. Gorelick, P. Greengard, *ibid.* **84**, 5710 (1987); C. M. Schworer, R. J. Colbran, J. R. Keefer, T. R. Soderling, *J. Biol. Chem.* **263**, 13486 (1988); L. L. Lou and H. Schulman, *J. Neurosci.* **9**, 2020 (1989).
11. S. G. Miller, B. L. Patton, M. B. Kennedy, *Neuron* **1**, 593 (1988).
12. The SRα expression vectors encoding α-CaM kinase or mutant CaM kinase were transfected into COS-7 cells [P. I. Hanson, M. S. Kapiloff, L. L. Lou, M. G. Rosenfeld, H. Schulman, *ibid.* **3**, 59 (1989)]. CaM kinase was purified by chromatography on DE-52, phosphocellulose, and calmodulin-Sepharose (*5*).
13. Y. L. Fong, W. L. Taylor, A. R. Means, T. R. Soderling, *J. Biol. Chem.* **264**, 16759 (1989). The Ala^{286} replacement was generated with a 23–base pair oligonucleotide (5′-GGC AGT CCA CGG CCT CCT GTCTG-3′) by standard procedures.
14. T. Yamauchi, S. Ohsaka, T. Deguchi, *ibid.*, p. 19108.
15. G. Thiel, A. J. Czernik, F. Gorelick, A. C. Nairn, P. Greengard, *Proc. Natl. Acad. Sci. U.S.A.* **85**, 6337 (1988).
16. R. P. Estep, K. A. Alexander, D. R. Storm, *Curr. Top. Cell. Regul.* **31**, 161 (1989); J. H. P. Skene, *Neurosci. Res. Suppl.* **13**, S112 (1990).
17. Binding data (or $K_{1/2}$ for activation, if binding data are not available) are from *Calmodulin*, P. Cohen and C. B. Klee, Eds. (Elsevier, Amsterdam, 1988); value for MARCKS was determined from peptide binding, J. M. Graff, T. N. Young, J. D. Johnson, P. J. Blackshear, *J. Biol. Chem.* **264**, 21818 (1989); data for the nonbacterial cyclase are from G. B. Rosenberg, A. V. M. Minocherhomjee, D. R. Storm, *Methods Enzymol.* **139**, 776 (1987).
18. Supported by GM24032 and MH45324 to L.S., GM 40600 to H.S., PHS training grant CA09302 to P.I.H., and a Swiss National Science Foundation fellowship to T.M.

4 November 1991; accepted 11 March 1992

A Mutant of TTX-Resistant Cardiac Sodium Channels with TTX-Sensitive Properties

Jonathan Satin,* John W. Kyle, Michael Chen, Peter Bell, Leanne L. Cribbs, Harry A. Fozzard, Richard B. Rogart

The cardiac sodium channel α subunit (RHI) is less sensitive to tetrodotoxin (TTX) and saxitoxin (STX) and more sensitive to cadmium than brain and skeletal muscle (μI) isoforms. An RHI mutant, with Tyr substituted for Cys at position 374 (as in μI) confers three properties of TTX-sensitive channels: (i) greater sensitivity to TTX (730-fold); (ii) lower sensitivity to cadmium (28-fold); and (iii) altered additional block by toxin upon repetitive stimulation. Thus, the primary determinant of high-affinity TTX-STX binding is a critical aromatic residue at position 374, and the interaction may take place possibly through an ionized hydrogen bond. This finding requires revision of the sodium channel pore structure that has been previously suggested by homology with the potassium channel.

Two classes of Na^+ channel subtypes (*1*) have been distinguished by their sensitivity to TTX and STX. Sodium channels in brain and innervated skeletal muscles that are TTX-sensitive (TTX-S) are blocked by nanomolar concentrations of TTX (*2*), whereas TTX-resistant (TTX-R) Na^+ channels in heart and denervated skeletal muscle are blocked by micromolar concentrations of TTX (*3, 4*). Molecular cloning and expression of Na^+ channel cDNAs show multiple isoforms of Na^+ channels that are encoded by a multigene family in mammals (*5*), where a difference in primary structure accounts for the possession of TTX-S or TTX-R properties (*6, 7*).

Molecular studies have provided information that locates the structural domain where TTX and STX bind to and block the Na^+ channel, thereby identifying the external entrance to the channel pore. The SS2 domain (Fig. 1) is a seven–amino acid segment that forms part of the external loop that connects membrane-spanning units S5 and S6. In the Brain II Na^+ channel, substitution of Glu^{387} with Gln in SS2 of the first (NH_2-terminal) repeat abolished sensitivity to TTX and STX (*8, 9*). In K^+ channels, mutagenesis of a region analogous to SS1 and SS2 (Fig. 1) modifies pore properties, including sensitivity to external blocking agents acting like TTX and STX (*10*).

Two of the seven amino acids in SS2 of the first NH_2-terminal repeat differ between the RHI (*11*) and the TTX-S Na^+ channel isoforms (Fig. 1). We mutated these two positions (*12*) to the corresponding amino acids found in the TTX-S skeletal muscle Na^+ channel isoform (μI). We determined the TTX and STX sensitivity for the RHI $Arg^{377} \rightarrow$ Asn mutant, where substitution of the positively charged Arg with a neutral Asn was predicted to restore TTX and STX sensitivity to the RHI Na^+ channel (*8*). The Na^+ current (I_{Na}) was elicited by a 7-ms depolarization to −10 mV in the presence of various concentrations of TTX (Fig. 2). Single-site dose-response curves for blockage of I_{Na} by toxin for the wild-type RHI and the $Arg^{377} \rightarrow$ Asn mutant are best fit with apparent dissociation constants (K_d) for TTX of 0.95 μM and 7.58 μM, respectively (Fig. 3A); the K_d's for STX are 91 nM and 184 nM, respectively. Thus, the

J. Satin and H. A. Fozzard, Laboratory of Cardiac Electrophysiology, Departments of Medicine and Pharmacological and Physiological Sciences, and The Committee on Cell Physiology, The University of Chicago, MC-6094, 5841 South Maryland Avenue, Chicago, IL 60637.
J. W. Kyle, M. Chen, P. Bell, L. L. Cribbs, R. B. Rogart, Laboratory of Molecular Neuro-Cardiology, Department of Medicine, and The Committee on Cell Physiology, The University of Chicago, MC-6094, 5841 South Maryland Avenue, Chicago, IL 60637.

*To whom correspondence should be addressed.

positively charged Arg^{377} does not account for the resistance of RHI to TTX and STX.

In the cardiac Na^+ channel, Cys^{374} is located two residues from the conserved Glu^{376} in the direction of the NH_2-terminus (11). In the μI isoform, the corresponding residue is an aromatic Tyr. Single-site dose-response curves for blockage of I_{Na} by toxin for wild-type RHI and its $Cys^{374} \rightarrow$ Tyr mutant are best fit with K_d's for TTX of 950 nM and 1.32 nM, respectively; K_d's for STX are 91.1 nM and 5.2 nM, respectively. These affinities for TTX and STX are similar to those of the TTX-S Na^+ channels.

A second characteristic that distinguishes native TTX-R cardiac from TTX-S Na^+ channels is their increased sensitivity to blockage by group IIB divalent cations such as Cd^{2+} and Zn^{2+} (13). These divalent cations also competitively inhibit TTX and STX binding (14), which suggests that they share a common binding site on Na^+ channels (15). About 30 times more Cd^{2+} was required to block the $Cys^{374} \rightarrow$ Tyr mutant (Fig. 3C) and about seven times less Cd^{2+} was required to block the $Arg^{377} \rightarrow$ Asn mutant than the wild-type RHI Na^+ channels.

A third characteristic that distinguishes TTX-R cardiac from TTX-S Na^+ channels is their use-dependent blockage by TTX in cardiac or skeletal muscles (4, 16) and in oocytes that express the cloned RHI (Fig. 4, A through C). We measured use-dependent blockage by stimulating oocytes with trains of depolarizations (7 ms) at 2 Hz. Control I_{Na} declined less than 10% for RHI and both mutants. With TTX present at half-block concentrations for resting channels, repetitive depolarization (2 Hz) further reduced I_{Na} by 47%, whereas neither mutant showed further blockage (Fig. 4, A through C). In contrast, with STX present, both mutant channels showed use-dependent blockage, with a rate that was fastest for the $Cys^{374} \rightarrow$ Tyr mutant, intermediate for the wild-type RHI, and slowest for the $Arg^{377} \rightarrow$ Asn mutant (Fig. 4, D through F). Both first pulse and use-dependent blockage (0.5 to 2 Hz) of $Cys^{374} \rightarrow$ Tyr channels are similar to that of native and cloned TTX-sensitive channels (17).

These mutations probably make structural changes in the binding site for TTX, STX, and Cd^{2+} that specifically alter only corresponding Na^+ channel functional properties because the $Cys^{374} \rightarrow$ Tyr and $Arg^{377} \rightarrow$ Asn substitutions both occur naturally in other Na^+ channel isoforms. Furthermore, the two mutations of the toxin binding site do not alter other properties such as kinetics for the I_{Na}'s (Table 1) or resistance to μ-conotoxin GIIIA (18), a blocker specific to the TTX-S skeletal muscle channel (19).

The TTX-S $Cys^{374} \rightarrow$ Tyr mutant is more sensitive to TTX than either the cloned μI or native TTX-S channels (Table 2). Furthermore, the $Cys^{374} \rightarrow$ Tyr mutant has an affinity for TTX greater than that for STX, which is contrary to that found in native and cloned Na^+ channels (Table 2). If we assume that the $Cys^{374} \rightarrow$ Tyr and $Arg^{377} \rightarrow$ Asn mutations affect toxin sensitivity, this double mutant of RHI would be expected to have K_d's within the range of the expressed μI I_{Na} in oocytes (Table 2). Complete reversion of the TTX-R RHI to TTX-S μI properties will require quantitation of toxin sensitivities for such combined mutants.

Previous hypotheses (20) that explain high-affinity TTX and STX binding in the Na^+ channel have focused on electrostatic attraction between the positively charged toxin guanidinium groups and negatively charged acidic groups in their Na^+ channel binding site. Support for this has come from the inhibition of toxin binding by mono-

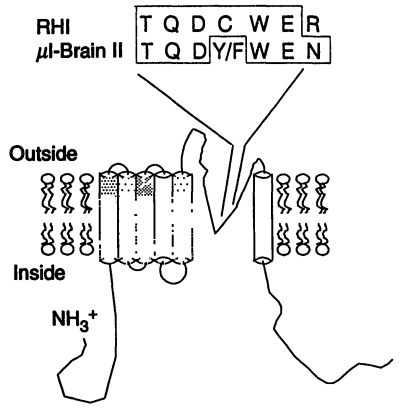

Fig. 1. Depiction of the first repeat of a generalized voltage-sensitive Na^+ channel. The seven–amino acid SS2 sequence is shown, and the differences between the TTX-R (RHI) and TTX-S (μI-Brain II) isoforms are indicated. All of the Na^+ channel isoforms, as well as most voltage-gated K^+ channels, share a common structural motif of six membrane-spanning segments repeated four times. A three-dimensional model of the Na^+ channel (27) places the region between transmembrane segment 5 and 6 within the plane of the membrane. We refer to the short segments between transmembrane segment 5 and 6 as SS1 and SS2 (27). Abbreviations for the amino acid residues are: C, Cys; D, Asp; E, Glu; F, Phe; N, Asn; Q, Gln; R, Arg; T, Thr; W, Trp; and Y, Tyr.

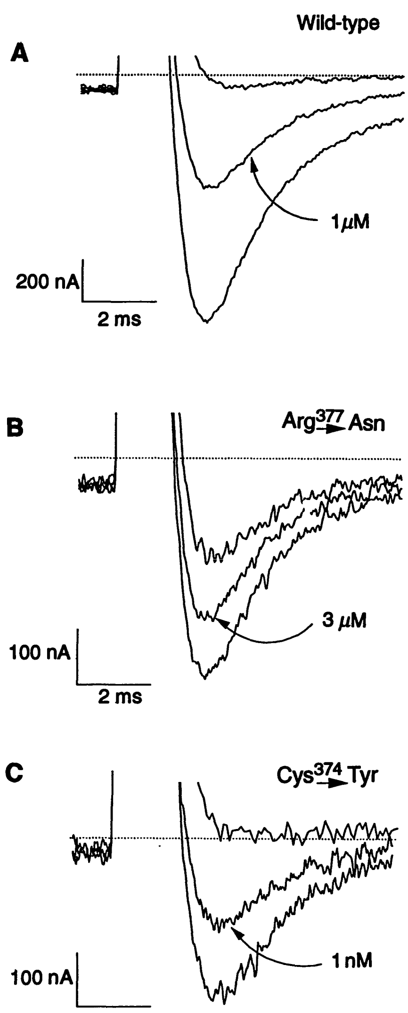

Fig. 2. Sodium currents from oocytes injected with expression vector that encodes (**A**) wild-type RHI, (**B**) $Arg^{377} \rightarrow$ Asn mutant, and (**C**) $Cys^{374} \rightarrow$ Tyr mutant. Currents were elicited by depolarizations to −10 mV from a holding potential of −100 mV. Oocytes (28) were held at a potential of −100 mV for at least 3 min before depolarizations in the presence of TTX to ensure that all channels were in the resting state. In (A), wild-type RHI; 0, 1, and 10 μM TTX; in (B), $Arg^{377} \rightarrow$ Asn; 0, 3, and 10 μM TTX; in (C), $Cys^{374} \rightarrow$ Tyr; 0, 1, and 10 nM TTX. Dashed line indicates no current.

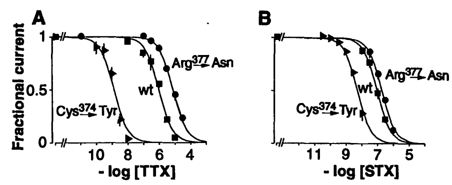

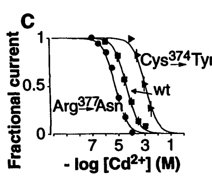

Fig. 3. Dose-response curves for the first pulse blockage of wild-type and SS2 mutant channels by TTX (**A**), STX (**B**), and Cd^{2+} (**C**). We measured the first pulse blockage by maintaining the holding potential at −100 mV for at least 200 s before V_{test}. The single-site curve is of the form

$$I_{Na,toxin}/I_{Na,control} = 1/\{1 + [toxin]/K_d\}$$

For TTX, the K_d's were 1.32 nM, 0.95 μM, and 7.58 μM for $Cys^{374} \rightarrow$ Tyr (triangles), wild-type RHI (squares) (wt), and $Arg^{377} \rightarrow$ Asn (circles), respectively. For STX, the K_d's were 5.2, 91.1, and 184 nM for $Cys^{374} \rightarrow$ Tyr, RHI, and $Arg^{377} \rightarrow$ Asn, respectively. In (C), K_d's were 1.22 mM, 43.3 μM, and 6.0 μM for $Cys^{374} \rightarrow$ Tyr, RHI, and $Arg^{377} \rightarrow$ Asn, respectively. Symbols represent the mean ± SEM.

valent and divalent cations and protons (2) and from the elimination of TTX and STX binding when anionic sites are removed from the Na^+ channel by COOH-modifying reagents (21) or with the point mutation $Glu^{387} \rightarrow Gln$ in the Brain II isoform (8). Also, two clusters of predominantly negatively charged amino acids in SS2 of all four internal repeats of the Brain II Na^+ channel were identified as major determinants of toxin binding (9).

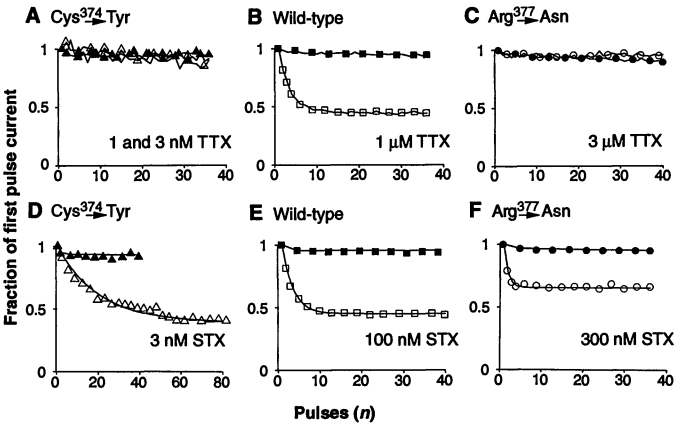

Fig. 4. Absence of use-dependent blockage by TTX of cardiac Na^+ channel mutants and altered rate of use-dependent blockage of cardiac Na^+ current by STX in SS2 mutants. Peak Na^+ currents normalized to the first pulse of a 2-Hz train of 7-ms depolarizations are plotted as a function of pulse number. **(A)** $Cys^{374} \rightarrow Tyr$; 0, 1, and 3 nM TTX; **(B)** wild-type RHI; 0 and 1 μM TTX; and **(C)** $Arg^{377} \rightarrow Asn$; 0 and 3 μM TTX. In (A) through (C), $V_{hold} = -100$ mV; $V_{test} = -10$ mV. In **(D)** through **(F)**, peak currents (symbols) are superimposed with a single exponential function with a time constant of 19.7 pulses for $Cys^{374} \rightarrow Tyr$ (D), 2.6 pulses for wild-type RHI (E), and 0.97 pulse for $Arg^{377} \rightarrow Asn$ (F). Note that the scale is expanded to 80 pulses for the $Cys^{374} \rightarrow Tyr$ data in (D). Symbol shapes are as in Fig. 3; closed symbols represent zero toxin and open symbols represent the indicated toxin concentration.

Table 1. Electrophysiological parameters of I_{Na} expressed in oocytes for the RHI and Na^+ channel mutants. τ (−10 mV) is the time constant of a single exponential function fitted to the decay of I_{Na} for a depolarization to −10 mV.

Channels	Availability*			Activation†			τ (−10 mV)	
	$V_{1/2}$	k	n	$V_{1/2}$	k	n	ms	n
$Cys^{374} \rightarrow Tyr$	−69.9 ± 3.6	5.02 ± 0.75	9	−31.7 ± 2.6	4.23 ± 0.69	9	2.1 ± 0.3	4
RHI	−72.2 ± 3.4	5.96 ± 1.06	14	−28.3 ± 4.4	5.24 ± 1.25	21	2.1 ± 0.3	7
$Arg^{377} \rightarrow Asn$	−70.0 ± 2.4	5.58 ± 1.28	8	−26.8 ± 3.0	4.97 ± 0.61	10	1.9 ± 0.2	4

*Availability is described by a Boltzmann distribution of the form $G_{Na} = 1/\{1+\exp(V_{hold} - V_{1/2})/k\}$, where $V_{1/2}$ is the midpoint and k is the slope. †Activation is described by a Boltzmann distribution of the form $G_{Na} = 1/\{1 + \exp(V_{1/2} - V_{test}/k\}$, where $V_{1/2}$ is the midpoint and k is the slope.

Table 2. Comparison of TTX and STX blockage of cloned cardiac, skeletal muscle, and wild-type Na^+ channels.

	K_{dTTX} (nM)	K_{dRHI}/K_d*	K_{dSTX} (nM)	K_{dRHI}/K_d*	K_{dTTX}/K_{dSTX}
		Cloned channels			
RHI	950	1	91.1	1	10
$Arg^{377} \rightarrow Asn$	7580	0.13	184	0.50	41
$Cys^{374} \rightarrow Tyr$	1.3	731	5.2	18	0.25
μI	40	24	3.0	30	14
		Native channels			
Cardiac/denervated skeletal muscle†	1518–2514	0.4–0.6	11.1–13.5	6.7–8	27–37
Denervated rat skeletal muscle‡	1000–3200	1–0.3			
Innervated skeletal muscle†	16	59	3.6	25	4.7
Innervated rat skeletal muscle‡	5.1–13	73–186			

*K_d of TTX or STX for the RHI wild-type/K_d of TTX or STX for the given channel type. †K_d determined from radiolabeled toxin binding (3). ‡K_d determined from I_{Na} recorded by a two-electrode voltage-clamp (29).

Our findings suggest a revision of the electrostatic model that explains TTX and STX binding. The interaction between toxin and critical aromatic amino acid residues in TTX-S Na^+ channels that align with RHI Cys^{374} is the primary force for high-affinity TTX and STX binding; electrostatic interactions have a secondary role. The $Cys^{374} \rightarrow Tyr$ mutant of RHI resulted in a 730-fold increase in affinity for TTX binding, which converted a low-affinity to a high-affinity toxin binding site, with the K_d for TTX reduced from the micromolar to the nanomolar range. In contrast, the two clusters of mainly anionic residues (9) were identified by mutations of the TTX-S Brain II Na^+ channel and resulted in a reduction of TTX affinity. Because these residues are conserved in RHI, they are unlikely to account for the observed difference between low- and high-affinity toxin binding sites. Further evidence against simple electrostatic attraction determining toxin affinity comes from the $Arg^{377} \rightarrow Asn$ RHI mutant. This mutation increases negative charge at the toxin binding site but decreases toxin affinity, which is contrary to the effect predicted by the electrostatic attraction. Other types of interactions that decrease toxin affinity must therefore be involved, such as steric hindrance, loss of potential covalent bonds (22), or hydrogen bonds with the dihydroxy groups of the C-12 moiety of STX (23).

The observed 730-fold increase in toxin binding affinity for the $Cys^{374} \rightarrow Tyr$ mutant requires an increase in binding energy of 3.9 kcal/mol, which is larger in size than that typically found for electrostatic attractions through space in biological proteins (24). An interaction with this magnitude of energy increase might occur through an ionized hydrogen bond between the positively charged guanidinium group in TTX and the corresponding Tyr in the $Cys^{374} \rightarrow Tyr$ RHI mutant and the μI Na^+ channel (25). The interaction between toxin and Tyr (perhaps along with other aromatic amino acids in SS2 domains from other repeats) is analogous to that proposed for binding of acetylcholine (ACh) with its biological binding sites (26). The primary binding force for ACh depends on a cation–π bond interaction between the quaternary ammonium of ACh with the electrons of aromatic amino acids (such as Tyr, Phe, and Trp) in the receptor, and electrostatic interactions are of secondary importance. Alternatively, replacement of the Cys^{374} may have removed a disulfide bond.

The similarity of external blockage of Na^+ channels by TTX and STX and of K^+ channels by charybdotoxin and tetraethyl ammonium (TEA) suggests that these agents occupy structurally homologous binding sites close to or within the mouth of the channel pore (*20*). Guy and Conti (*27*) and Hille (*20*) suggested an alignment of amino acid sequences where the Glu^{376} involved in TTX and STX binding in Na^+ channels is one to two positions away from the critical residue at position 449 in K^+ channels, a major site in charybdotoxin and TEA binding. Our results with the $Cys^{374} \rightarrow Tyr$ and the $Arg^{377} \rightarrow Asn$ mutants demonstrate that residues 374 to 377 are essential for binding of TTX and STX and Cd^{2+}, which would align with residues 444 to 447 of the *Shaker* K^+ channel (*20, 27*). This would place the TTX and STX receptor about three-eighths to three-quarters of the way into the pore, which is inconsistent with the observed lack of voltage dependence for TTX and STX binding. Identification of the residue at position 374 as critical to high-affinity toxin binding reveals the structural difference that distinguishes TTX-R and TTX-S Na^+ channel isoforms and explains the high-affinity divalent cation blockage of the RHI and the competition of divalent ions and toxin for binding. The position of this residue may require revision of the Na^+ channel pore structure suggested by homology with the K^+ channel.

Note added in proof: $Cys^{374} \rightarrow Phe$ has the same properties as $Cys^{374} \rightarrow Tyr$.

REFERENCES AND NOTES

1. R. Barchi, *Trends Neurosci.* **10**, 221 (1987); R. B. Rogart, *Annu. Rev. Physiol.* **43**, 711 (1981).
2. J. M. Ritchie and R. Rogart, *Rev. Physiol. Biochem. Pharmacol.* **79**, 1 (1977).
3. J. F. Renaud *et al.*, *J. Biol. Chem.* **258**, 8799 (1983); R. B. Rogart, *Ann. N.Y. Acad. Sci.* **479**, 402 (1986).
4. C. J. Cohen *et al.*, *J. Gen. Physiol.* **78**, 383 (1981).
5. J. S. Trimmer and W. S. Agnew, *Annu. Rev. Physiol.* **51**, 401 (1989).
6. L. L. Cribbs *et al.*, *FEBS Lett.* **275**, 195 (1990).
7. M. White *et al.*, *Mol. Pharmacol.* **39**, 604 (1991).
8. M. Noda *et al.*, *FEBS Lett.* **259**, 213 (1989).
9. H. Terlau *et al.*, *ibid.* **293**, 93 (1991).
10. R. MacKinnon and G. Yellen, *Science* **250**, 276 (1990).
11. R. B. Rogart *et al.*, *Proc. Natl. Acad. Sci. U.S.A.* **86**, 8170 (1989).
12. To construct the mutants, we created a fragment by the polymerase chain reaction (PCR) that encompassed the Bgl II restriction sites at nucleotides (nt) 197 and 1162. The 5′ primer bound to the 5′ side of nt 197, and the 3′ primer included the Bgl II site at nt 1162 and also incorporated a single- or double-nucleotide mutation that resulted in a single amino acid change upon translation. The PCR product was ligated to a subclone (pRH11-71) of the rat cardiac Na^+ channel that spanned nt 445 to 2971. The Nsi I (nt 553) to Bam HI (nt 2956) fragment was then isolated and ligated into the expression vector pXOI. For transcription, templates were linearized with Xba I and transcribed with T7 RNA polymerase. Reaction conditions were described (*6*). Reagents were from Stratagene.
13. C. Frelin *et al.*, *Eur. J. Pharmacol.* **122**, 245 (1986); D. DiFrancesco *et al.*, *Proc. R. Soc. London Ser. B* **223**, 475 (1985); D. A. Hanck and M. F. Sheets, *J. Physiol.* (*London*), in press.
14. J. Reed and W. Raftery, *Biochemistry* **15**, 944 (1976); R. L. Barchi and J. B. Weigele, *J. Physiol.* (*London*) **295**, 383 (1979); W. N. Green, L. B. Weiss, O. S. Andersen, *J. Gen. Physiol.* **89**, 873 (1987).
15. L. Schild and E. Moczydlowski, *Biophys. J.* **59**, 523 (1991).
16. E. Carmeliet, *ibid.* **51**, 109 (1987); P. M. Vassilev *et al.*, *Am. J. Physiol.* **251**, H475 (1986); R. Eickhorn *et al.*, *Pfluegers Arch.* **416**, 398 (1990).
17. U. Lonnendonker, B. Neumcke, R. Stampfli, *Pfluegers Arch.* **416**, 750 (1990); V. L. Salgado, J. Z. Yeh, T. Narahashi, *Ann. N.Y. Acad. Sci.* **479**, 84 (1986); D. E. Patton and A. L. Goldin, *Neuron* **7**, 637 (1991).
18. J. Satin, unpublished data.
19. G. Strichartz, T. Rando, G. K. Wang, *Annu. Rev. Neurosci.* **10**, 237 (1987).
20. B. Hille, *Ionic Channels of Excitable Membranes* (Sinauer, Sunderland, MA, ed. 2, 1992); *Biophys. J.* **15**, 615 (1975).
21. B. C. Spalding, *J. Physiol.* (*London*) **305**, 485 (1980); P. Shrager and C. Profera, *Biochim. Biophys. Acta* **318**, 141 (1973).
22. G. Strichartz *et al.*, *Ann. N.Y. Acad. Sci.* **479**, 96 (1986).
23. S. L. Hu and C. Y. Kao, *J. Gen. Physiol.* **97**, 561 (1991).
24. R. MacKinnon and C. Miller, *Science* **245**, 1382 (1989). These authors estimated for the electrostatic interaction of charybdotoxin with the K^+ channel that a single charge alteration reduces affinity 3.5 times, which is equivalent to a free-energy change of 0.7 kcal/mol.
25. C. Branden and J. Tooze, *Introduction to Protein Structure* (Garland, New York, 1991). For instance, the ionized hydrogen bond between Tyr^{169} of tyrosyl-tRNA synthetase and its positively charged substrate contribute about 3.7 kcal/mol.
26. D. A. Dougherty and D. A. Stauffer, *Science* **250**, 1558 (1990).
27. H. R. Guy and F. Conti, *Trends Neurosci.* **13**, 201 (1990).
28. Oocytes were injected with 50 to 150 ng of cRNA. Whole-oocyte current was recorded with a two-electrode voltage-clamp (TEV-200, Dagan) 2 to 5 days after injection. Recordings were made at 20° to 22°C in a flowing bath solution that consisted of 90 mM NaCl, 2.5 mM KCl, 1 mM $CaCl_2$, 1 mM $MgCl_2$, and 10 mM Hepes (pH 7.4). $CdCl_2$ was added to the bath from a 100 mM stock solution. TTX and STX were purchased from Calbiochem.
29. P. A. Pappone, *J. Physiol.* (*London*) **306**, 377 (1980); T. Gonoi, S. J. Sherman, W. A. Catterall, *J. Neurosci.* **5**, 2559 (1985).

30. We thank G. Mandel for the gift of μI cDNA; A. Fox for help with Axobasic 1.0; T. Larsen and N. Soares for technical assistance; and D. Hanck and J. Makielski for helpful discussions. Supported by NIH grants HL-20592, HL-37217, and NS 23360, a grant from the Upjohn Company, and a grant from the International Life Sciences Institute.

17 January 1992; accepted 31 March 1992

Identification of Heregulin, a Specific Activator of $p185^{erbB2}$

William E. Holmes,* Mark X. Sliwkowski, Robert W. Akita, William J. Henzel, James Lee, John W. Park, Daniel Yansura, Nasrin Abadi, Helga Raab, Gail D. Lewis, H. Michael Shepard,† Wun-Jing Kuang, William I. Wood, David V. Goeddel, Richard L. Vandlen*‡

The proto-oncogene designated *erb*B2 or HER2 encodes a 185-kilodalton transmembrane tyrosine kinase ($p185^{erbB2}$), whose overexpression has been correlated with a poor prognosis in several human malignancies. A 45-kilodalton protein heregulin-α (HRG-α) that specifically induced phosphorylation of $p185^{erbB2}$ was purified from the conditioned medium of a human breast tumor cell line. Several complementary DNA clones encoding related HRGs were identified, all of which are similar to proteins in the epidermal growth factor family. Scatchard analysis of the binding of recombinant HRG to a breast tumor cell line expressing $p185^{erbB2}$ showed a single high affinity binding site [dissociation constant (K_d) = 105 ± 15 picomolar]. Heregulin transcripts were identified in several normal tissues and cancer cell lines. The HRGs may represent the natural ligands for $p185^{erbB2}$.

The $p185^{erbB2}$ protein is a 185-kD transmembrane tyrosine kinase encoded by the erbB2 proto-oncogene (*1*) that is similar to the epidermal growth factor (EGF) receptor (*2*) and the HER3, or c-*erb*B3, protein (*3*). Both $p185^{erbB2}$ and the EGF receptor are associated with certain human malignancies (*4*). In particular, overexpression of $p185^{erbB2}$ correlates with a poor prognosis in breast, ovarian, gastric, and endometrial cancers and non-small cell lung adenocarcinoma (*5*). EGF and transforming growth factor–α (TGF-α), which are ligands for the EGF receptor, clearly promote cell growth and transformation (*1, 6*). However, a similar dependence on a ligand for growth or transformation in cells expressing $p185^{erbB2}$ has not been established. Neither EGF nor TGF-α binds to or activates $p185^{erbB2}$ (*7*).

Evidence that $p185^{erbB2}$ may respond to exogenous ligands includes observations

Departments of Protein Chemistry, Molecular Biology and Cell Biology, Genentech, Inc., South San Francisco, CA 94080.

*W. E. Holmes and R. L. Vandlen are equal contributors to this work.
†Present address: Canji Pharmaceuticals, San Diego, CA 92121.
‡To whom correspondence should be addressed.